A Quasi Quantum Treatment of inelastic molecular collisions

A. Ballast*, A. Gijsbertsen*, H. Linnartz†, C. A. Taatjes** and S. Stolte*,‡

*Laser Centre and Department of Physical Chemistry, Vrije Universiteit Amsterdam,
De Boelelaan 1083, 1081 HV Amsterdam, The Netherlands
†Sackler laboratory for Astrophysics, Leiden Observatory,
P.O. Box 9513, 2300 RA Leiden, The Netherlands
**Combustion Research Facility, Mailstop 9055, Sandia National Laboratories,
Livermore, CA 94550, USA
‡Correspondence should be addressed to this author, fax +31 20 5987643, e-mail stolte@few.vu.nl

Abstract. A Quasi Quantum Treatment is used to describe the collisions of He with state selected NO molecules ($j = \frac{1}{2}$, $\overline{\Omega} = \frac{1}{2}$, $\varepsilon = -1$). This leads to a propensity rule. The angular dependence of the cross sections for excitation to states with neighboring rotational angular momentum quantum number j' and with the same parity is shown to be similar except for a pre-factor. Experimental results support this rule. Unlike conventional quantum mechanical (or semiclassical) treatments, QQT requires no summation over the orbital angular momentum quantum number l or integration over the impact parameter b. This eliminates the need to solve large sets of coupled differential equations that couple l and rotational state channels among which interference can occur. The QQT provides a physical interpretation of the scattering amplitude, that is represented by a Legendre moment and a phase shift factor. Application of the QQT for a simple hard-shell potential predicts an angular dependence of the collision cross-section that corresponds surprisingly well to the experimental and full quantum mechanical results.

Keywords: differential cross-sections, molecular-collisions, NO collisions, rotational-excitation, potential-energy surface, kinetic-theory model
PACS: 34.50.Pi, 34.20.Mq, 82.20.Fd, 39.10.+j

INTRODUCTION

In order to understand (and eventually predict and control) macroscopic chemical reactions, it is necessary to understand single encounters between molecules or molecules and atoms [1]. Recent work [2] describes and discusses a Quasi Quantum Treatment (QQT) that was developed to provide insight into inelastic collisions and to allow for rapid quantitative calculations. Although the outcome of a relatively simple collision process - for example a He-NO collision - can be calculated up to a reasonable degree using full quantum mechanical methods, these calculations are computationally demanding and do not offer much insight in the actual physics behind it. For example, the rare gas - NO orientational dependence of the collision cross section on the final rotational state [3] could be reproduced using close-coupling calculations, but the origin of this behavior remained unexplained. The Quasi Quantum Treatment (QQT) provides a powerful tool for understanding collisions and for drawing several quantitative conclusions without the large numerical effort of close-coupling methods. It explains (and reproduces) the oscillatory behavior of the steric asymmetry as function of the final rotational state [4] as well as the parity-pair effects that are observed in the differential cross sections for He-NO and D_2-NO collisions [5].

This paper is organized in 5 sections. The Theory section describes the main ideas behind the QQT and explains how it relates to other theoretical methods. Furthermore QQT is applied to fully state selected, non-oriented molecules. A hard shell approximation is used to obtain the molecule fixed scattering amplitude. This scattering amplitude, that contains the phase shift, is necessary to obtain quantitative results from the QQT. In the Experimental section a short description of recent He-NO scattering experiments [6] is given. In the Results and Discussion section the QQT results are compared to experimental and to close-coupling differential cross sections. Conclusions and a future outlook are given in the Concluding Remarks section.

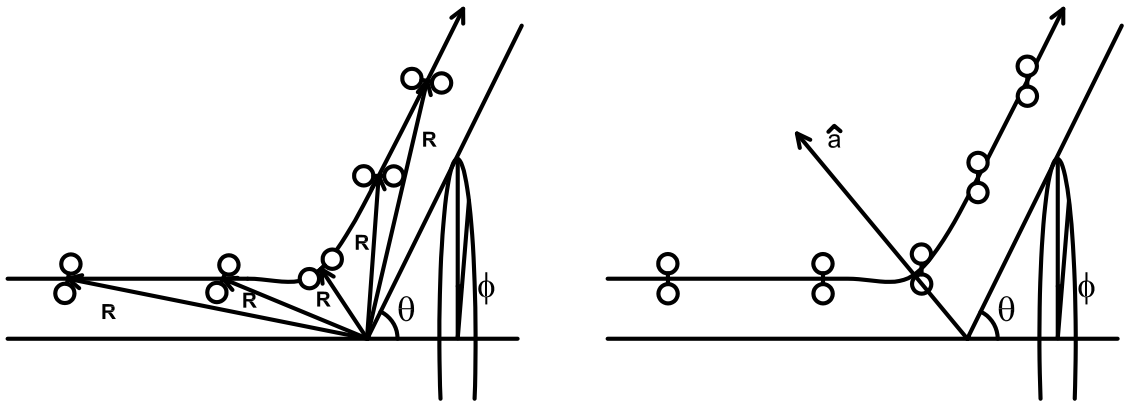

Figure 1. To illuminate the differences between the IOS approximation (left panel) and the QQT approach (right panel) the trajectory of a NO molecule scattering from the origin (a He atom) is given. The NO molecule is coming from the left with impact parameter b and is scattered in the direction specified by the spherical angles θ and ϕ. The IOS approximation assumes the molecular orientation to be fixed with respect to the intermolecular distance **R**, rotating the molecule in a fixed way, irrespective of the physics involved. The QQT approach, on the other hand, only assumes that the orientation of the molecule does not change during the time of impact. This leads to a more realistic picture. Instead of specifying the impact parameter, the QQT approach specifies the direction of the momentum transfer, or kinematic apse $\hat{\mathbf{a}}$.

THEORY

The conventional exact close coupling solution of the scattering problem of a rare gas atom and a hetero nuclear rigid diatomic requires the expansion of the incoming plane wave into an infinite sum of spherical waves. To solve the He-NO inelastic scattering problem at $E_{tr} \approx 500\ \mathrm{cm}^{-1}$, one has to solve a large set (typically 1300) of coupled differential equations for each value of the total angular momentum J and parity [7]. The maximum value of J is typically 120.5. These conventional quantum treatments provide good quantitative results, but yield little insight into the actual physics behind phenomena and their behavior under different circumstances. Their long calculation times are not well-suited for trying out many different values of the input parameters.

To circumvent the above-mentioned disadvantages, a large number of approximate methods have been developed. Among these, the semi classical version of the Infinite Order Sudden approximation (IOS) has turned out to be particularly useful. In this approximation the collision of an atom with a diatomic is described using a reference frame in which the molecular axis is assumed to remain fixed with respect to the intermolecular distance, see Fig. 1. The IOS approximation can yield satisfactory results in the calculation of m,m' degeneracy averaged collision cross sections, but is well known to err in predicting the m,m' dependence. Here m,m' denote the projection, before and after the collision, of the total angular momentum on a space fixed axis.

Khare et al. [8, 9] showed that there is a strong propensity for preserving the projection of the rotational angular momentum when using the kinematic apse as the quantization axis. This cannot be incorporated into the infinite order sudden approximation, because the quantization axis is chosen along the intermolecular distance. By replacing the sum over the orbital angular momentum numbers l (or the integral over the impact parameters b) by an integral over the angular variables specifying the direction of the momentum transfer [10–12], and by assuming conservation of the angular momentum component along the kinematic apse, we can obtain a formulation that leads to a significant reduction in computation time with respect to the close coupled calculations, while still providing reasonably accurate results. This QQT approach is therefore a major improvement over the common IOS approach.

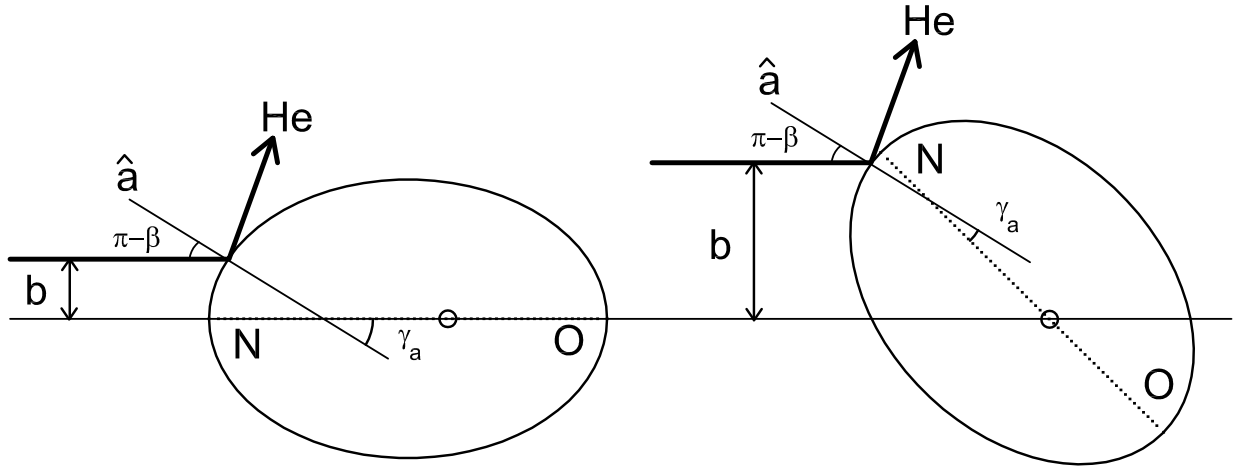

Figure 2. All orientations are present in the wave function. Constructive and destructive interference between the scattered waves will occur depending on the difference in path length. The potential can cause scattering under a certain angle for a whole range of impact parameters. Note that for a hard shell as drawn here, the kinematic apse $\hat{\mathbf{a}}$ coincides with the surface normal $\hat{\mathbf{n}}$.

Quasi Quantum Treatment

The QQT aims at the simplification and approximation of exact quantum treatments. It presents an intuitive basis for understanding the relation between inelastic collisions and the anisotropy of the inter-molecular potential. Instead of a partial wave expansion approach, we take a kind of Feynman path integral approach, but in the limit of geometric optics, where the DeBroglie wavelength is much smaller than the size of the object. In this way diffraction effects - that dominate for forward scattering angles - are not taken into account [13]. We retain however the interference effects caused by the anisotropy of the PES: a quantum state of NO can be seen as a superposition of different orientations. Because of the path length differences caused by the anisotropy of NO the scattering contributions from the different orientations will interfere. See Fig. 2.

To reduce the complexity of the calculations, we assume that the projection of the rotational angular momentum of the NO molecule on the kinematic apse [8, 9] is conserved during the collision. This is a reasonable assumption, since classically no torque is exerted on this axis, the change of momentum being in the direction of this axis. Reasonable differential cross sections (quantized in the collision frame) can be obtained by calculating and transforming only the $\Delta m = 0$ scattering amplitude from the kinematic apse frame for a given $j \rightarrow j'$ transition [9, 14].

The kinematic apse is defined as

$$\mathbf{a} = \mathbf{k}' - \mathbf{k}, \quad \hat{\mathbf{a}} = \frac{\mathbf{k}' - \mathbf{k}}{|\mathbf{k}' - \mathbf{k}|} \tag{1}$$

The spherical angles which define the direction of the kinematic apse in the collision frame ($\hat{\mathbf{Z}} \equiv \hat{\mathbf{k}}$) are defined as β and α (with $\frac{1}{2}\pi \leq \beta \leq \pi$ and $0 \leq \alpha \leq 2\pi$). The orientation of the molecular axis ($\hat{\mathbf{z}}$) with respect to the kinematic apse is given by the spherical angles γ_a and ϕ_a. The direction of the outgoing momentum $\hat{\mathbf{k}}'$ with respect to the direction of the incoming momentum $\hat{\mathbf{k}}$ is given by the spherical angles θ and φ. For inelastic collisions $k' \leq k$. The allowed values of k' follow from the rotational energy levels $E(j)$ of the NO-molecule. The amount of kinetic energy that is converted into rotation is

$$E(j') - E(j) = \frac{\hbar^2}{2\mu}(k^2 - k'^2) \tag{2}$$

where μ is the reduced mass of the collision system.

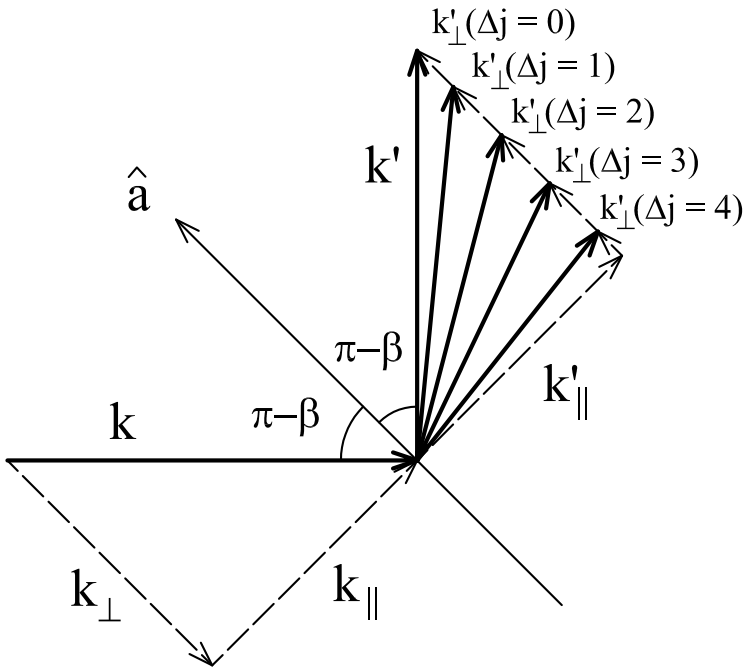

Figure 3. For a hard shell, the scattering angle is defined by only the incoming momentum, the surface normal $\hat{\mathbf{n}}$ (that coincides with the kinematic apse $\hat{\mathbf{a}}$) and the rotational excitation $\Delta j = j' - j$.

We will neglect the (small) attractive part of the rare gas - NO interaction and we will only consider spin-orbit conserving $\Omega' = \Omega$ transitions. The spin orbit changing transitions are mainly due to the difference PES V_{diff} [15] and that is not included in the present treatment.

The conventional scattering amplitude $f_{j,m,\bar{\Omega},\varepsilon\to j',m',\bar{\Omega}',\varepsilon'}(\theta,\varphi)$ gives the amplitude for scattering in the direction of $\mathbf{k}'$. Its angular dependence is expressed in terms of the spherical angles θ and φ with respect to $\mathbf{k}$. Instead, we introduce a scattering amplitude $g_{j,m,\bar{\Omega},\varepsilon\to j',m',\bar{\Omega}',\varepsilon'}(\beta,\alpha)$. Instead of specifying the direction of $\mathbf{k}'$ it specifies the direction of $\mathbf{a}$ using the spherical angles β and α with respect to $\mathbf{k}$. Given a specific j and j', the mapping between $\mathbf{a}$ and $\mathbf{k}'$ is unique (see Fig. 3). This change of variables also affects the respective elements of solid angle $d\omega$ and $d\omega_a$, introducing a Jacobian $d\omega/d\omega_a$. The azimuthal angles α and φ are redundant because of cylindrical symmetry, and one should note that $\alpha = \varphi$. The dimensionless scattering amplitudes f and g are related as follows

$$d\sigma = \frac{1}{k^2}|f(\theta)|^2 d\omega = \frac{1}{k^2}\left[|f(\theta(\beta))|^2 \frac{d\omega}{d\omega_a}\right] d\omega_a = \frac{1}{k^2}|g(\beta)|^2 d\omega_a \tag{3}$$

with the Jacobian

$$\frac{d\omega}{d\omega_a} = \frac{\sin\theta d\theta}{\sin\beta d\beta} \tag{4}$$

The scattering amplitude in the apse frame (with the kinematic apse $\hat{\mathbf{a}}$ also serving as the quantization axis) is defined as: (with $m_a' = m_a$ and $\Omega' = \Omega$, as said before)

$$\begin{aligned} g_{jm_a\bar{\Omega}\varepsilon\to j'm_a\bar{\Omega}\varepsilon'}(\beta) &= C(\beta)\ \langle j'm_a\bar{\Omega}\varepsilon'|\ \tilde{g}(\beta)\ |jm_a\bar{\Omega}\varepsilon\rangle \\ &= C(\beta)\iint \langle j'm_a\bar{\Omega}\varepsilon'|\hat{\mathbf{z}}'\rangle\langle\hat{\mathbf{z}}'|\ \tilde{g}(\beta)\ |\hat{\mathbf{z}}\rangle\langle\hat{\mathbf{z}}|jm_a\bar{\Omega}\varepsilon\rangle\, d\hat{\mathbf{z}}d\hat{\mathbf{z}}' \\ &= C(\beta)\iint \langle j'm_a\bar{\Omega}\varepsilon'|\hat{\mathbf{z}}'\rangle\ g_{\hat{\mathbf{z}}'\hat{\mathbf{z}}}(\beta)\delta(\hat{\mathbf{z}}',\hat{\mathbf{z}})\ \langle\hat{\mathbf{z}}|jm_a\bar{\Omega}\varepsilon\rangle\, d\hat{\mathbf{z}}d\hat{\mathbf{z}}' \\ &= C(\beta)\int g_{\hat{\mathbf{z}}}(\beta)\ \langle j'm_a\bar{\Omega}\varepsilon'|\hat{\mathbf{z}}\rangle\langle\hat{\mathbf{z}}|jm_a\bar{\Omega}\varepsilon\rangle\, d\hat{\mathbf{z}} \\ &= C(\beta)\int_0^{\pi}\int_0^{2\pi} g(\gamma_a;\beta)\ \Psi^*_{j'm_a\bar{\Omega}\varepsilon'}(\gamma_a,\phi_a)\ \Psi_{jm_a\bar{\Omega}\varepsilon}(\gamma_a,\phi_a)\ \sin\gamma_a\, d\phi_a d\gamma_a \end{aligned} \tag{5}$$

where $C(\beta)$ is a normalization factor that will be discussed later. The third equal sign uses a sudden approximation: the orientation of the NO-molecule does not change significantly during the collision process. The scattering amplitude for the molecule oriented into a specific direction (molecule fixed scattering amplitude) $g(\gamma_a;\beta)$ depends on $\mathbf{a}$, not only on $\hat{\mathbf{a}}$, and can therefore be written as $g_{\hat{\mathbf{z}}}(\mathbf{a})$ or $g_{j\to j'}(\gamma_a;\beta)$.

To evaluate (5), we assume a hard shell PES, see table 2 in [2]. The molecule fixed scattering amplitude $g_{j\to j'}(\gamma_a;\beta)$ is for one orientation only (specified value of γ_a). This means that the associated differential cross-section $|g_{j\to j'}(\gamma_a;\beta)|^2$ does not involve any interference between different trajectories. This differential cross-section is therefore equal to the classical differential cross-section (given the facts that we use classical trajectories and that the classical differential cross-section for a hard shell is independent of j' in the sudden approximation, classically j' depends on the rotational inertia). We will write

$$g_{j\to j'}(\gamma_a;\beta) = |g|e^{i\arg(g)} = g_{class}(\gamma_a;\beta)e^{i\eta_{j\to j'}(\gamma_a;\beta)} \tag{6}$$

Because of the anisotropy of the PES the path length of the trajectories is orientation dependent. Using the DeBroglie wavelength these path length differences will result in phase differences. Assigning a phase difference of zero to the virtual trajectory through the origin we can write

$$\eta_{j\to j'}(\gamma_a;\beta) = \mathbf{R}_c\cdot\mathbf{a} \tag{7}$$

Here $\mathbf{R_c}$ is the distance from the origin to the point of contact. The phase η depends on $\mathbf{a}$ and therefore on $j\to j'$. Scattering from a superposition of orientations will result in interference between trajectories (scattered by those different orientations) that have the same initial and final state. Two trajectories having the same initial state will interfere if and only if they share the same $\mathbf{a}$ (not $\hat{\mathbf{a}}$). Classically there is only one $\mathbf{a}$ for every $\hat{\mathbf{a}}$; in our QQT approach there are several $\mathbf{a}$ for every $\hat{\mathbf{a}}$: one for every energetically allowed j'. We would like the sum of all differential cross-sections that share the same $\hat{\mathbf{a}}$ to be equal to the classical differential cross-section. The factor $C(\beta)$ is therefore chosen such that

$$|g_{class}(\beta)|^2 = \int |\psi_{jm_a\bar{\Omega}\varepsilon}|^2|g_{class}(\gamma_a;\beta)|^2 d\hat{\mathbf{z}} = C^2(\beta)\sum_{j',\varepsilon'}\left|\int \psi^*_{j'm_a\bar{\Omega}\varepsilon'}\, g_{j\to j'}(\gamma_a;\beta)\,\psi_{jm_a\bar{\Omega}\varepsilon}d\hat{\mathbf{z}}\right|^2 \tag{8}$$

The classical molecule fixed scattering amplitude in the apse frame follows from

$$\frac{d\sigma}{d\omega_a} = \frac{1}{k^2}|g_{class}(\gamma_a;\beta)|^2 \tag{9}$$

We start with the element of solid angle $d\omega_a = d\beta\cdot\sin\beta d\alpha$. The intersection of this "cone" with the hard shell gives us the element of scattering surface dA. This dA presents an area to the incoming beam of $|\hat{\mathbf{k}}\cdot\hat{\mathbf{n}}|dA = |\cos\beta|dA = d\sigma$. On a sphere this $d\omega_a$ has an area dA of $\rho^2 d\omega_a = \rho d\beta\cdot\rho\sin\beta d\alpha$. On a general surface this $d\omega_a$ has an area dA of $\rho_1 d\beta\cdot\rho_2\sin\beta d\alpha = \rho_1\rho_2 d\omega_a$, where ρ_1,ρ_2 are the radii of curvature of the surface at (β,α) in the direction of $d\beta$ and $d\alpha$ respectively. A helpful image is that of a torus or bicycle tyre.[1] Now we have

$$d\sigma = \rho_1\rho_2|\cos\beta|d\omega_a, \quad \text{and therefore} \quad g_{class}(\gamma_a;\beta) = k\sqrt{\rho_1(\gamma_a)\rho_2(\gamma_a)|\cos\beta|} \tag{10}$$

[1] For a point on the outside of the tyre, where it touches the road, ρ_1 is the radius of the tyre (or wheel) and ρ_2 is the radius of the tube (half the thickness of the tyre). Now consider the scattering of light from a rectangular piece of silvery paper that sticks to the tyre.

Note that ϕ_a, the azimuthal angle around $\hat{\mathbf{a}}$, is redundant.

Using the above results and writing the product of the wave functions in (5) as a sum of rotation matrices of which only one term survives, we obtain for $j=\frac{1}{2}, \overline{m}_a=\frac{1}{2}, \overline{\Omega}=\frac{1}{2}$, and $\varepsilon=-1$ to $j', \overline{m}_a=\frac{1}{2}, \overline{\Omega}=\frac{1}{2}$, and ε' the differential cross section:

$$\frac{d\sigma_{j',\varepsilon'}}{d\omega} = C(\beta)^2 \frac{j'+\frac{1}{2}}{4k^2} \frac{\sin\beta}{\sin\theta} \left|\frac{\partial\beta}{\partial\theta}\right| \; |g_{j'+\varepsilon'/2}(\beta)|^2 \tag{11}$$

$$\text{with:} \qquad g_n(\beta) = \int_{-1}^{1} g_{j\to j'}(\gamma_a;\beta) P_n(\cos\gamma_a) d\cos(\gamma_a)$$

Note that $n = j' + \varepsilon'/2$. From (11) it follows that the differential cross sections for j', ε' and for $j'+\varepsilon', -\varepsilon'$ have the same form: they differ by a factor that is independent of β (or θ), assuming $g_{j\to j'}(\gamma_a;\beta)$ (i.e. $\eta_{j\to j'}(\gamma_a;\beta)$) to be weakly dependent on j'. We label each "form" with the order n of the Legendre polynomial in (11) and refer to such a pair of similar differential cross sections as a parity pair, because the final states have the same parity $p=(-1)^{j-\varepsilon/2}$. Within a parity pair we have a $j'=n-\frac{1}{2}$ and a $j'=n+\frac{1}{2}$. The differential cross section for the larger j' is larger than the differential cross section for the smaller j' by a factor of $\frac{n+1}{n}$.

EXPERIMENTS

Differential cross sections can be observed experimentally and provide a good test for theoretical scattering calculations. The velocity-mapped ion-imaging technique [16] is a convenient method to obtain these cross sections. It is nowadays commonly used in the field of molecular dynamics [17–25], and allows one to rapidly measure the velocity distribution of molecules or fragments after an event like a collision or a photodissociation provided a usable ionization scheme exists. The crossed molecular beam machine used in the experiments has been described in detail in [6] and only some of the most relevant conditions are mentioned in the following.

A beam of 16 % NO seeded in Ar expands from a General Valve. Due to adiabatic cooling, most of the NO molecules are in their rotational ground state with rotational quantum number $j=\frac{1}{2}$. After expansion, the NO beam enters a 1.6 meter long hexapole state selector. The hexapole focusses the molecules in the low field seeking upper component of the λ-doublet ($j=\frac{1}{2}, \overline{\Omega}=\frac{1}{2}, \varepsilon=-1$) into the collision region and diverges molecules in the high field seeking lower component ($j=\frac{1}{2}, \overline{\Omega}=\frac{1}{2}, \varepsilon=1$). Molecules in higher rotational states are much less affected by the hexapole. The parameter ε denotes the symmetry index, while $\overline{\Omega}$ ($=|\Omega|$) is the (absolute value of the) projection of the electronic angular momentum onto the molecular axis. The hexapole increases the amount of $j=\frac{1}{2}, \overline{\Omega}=\frac{1}{2}, \varepsilon=-1$ molecules in the collision region by a factor of 70. The hexapole focussed beam of NO molecules ($v_{NO}=593$ m/s) is crossed in the collision chamber by a beam of He atoms ($v_{He}=1760$ m/s). These velocities result in a nominal collision energy of 514 cm^{-1} [6]. An encounter of a He atom with a NO molecule might induce rotation of the NO. Energetically it is allowed to excite the NO molecules up to $\Delta j = j'-j = 16$. The rotationally excited NO molecules are ionized via a (1+1') resonance enhanced multi photon ionization (REMPI) scheme [26] along the electronic $A\,^2\Sigma^+ \leftarrow X\,^2\Pi$ transition using an excimer (XeCl) pumped dye laser with a bandwidth of about 0.1 cm^{-1}. The NO molecules are excited using tunable light of ≈ 226 nm and are subsequently ionized using the 308 nm light of the excimer laser. Velocity-mapped ion-imaging is applied to obtain the two dimensional velocity distribution of the scattered NO molecules.

To suppress contributions from other ionized molecules (oil or water) to the ion images, time-of-flight (TOF) gating is applied. The contributions to the images of thermal NO and of non-colliding NO molecules in the NO beam at the collision center are minimized by subtracting background images. The He beam is switched from "on" to "off" after every 100 laser shots. This procedure is repeated typically 20 times. The images with the He beam "off" are subtracted from those with the He beam "on". As the excimer/dye laser system and General Valves run at 10 Hz, collecting an image takes approximately 7 minutes.

To indicate the experimental geometry, the left panel of Fig. 4 shows an ion-image that was collected with the dye laser tuned to the $j=\frac{1}{2}, \overline{\Omega}=\frac{1}{2}, \varepsilon=-1$ NO ground state. Some (1%) of NO was added to the He beam to visualize it. The white spots indicate the positions where the NO molecules hit the detector after being ionized and accelerated towards the detector. This immediately provides the velocity distribution of the He and the Ar/NO beam. Together, these velocities form the basis of the Newton diagram that is drawn in the right panel of Fig. 4. The ion images that are shown in the remainder of this work consist only of the square around the Newton scattering sphere in Fig. 4.

Differential cross sections are extracted from the ion images as described in [6]. Collision-induced rotational alignment, the detection probability due to different residence times for slow and fast molecules within the detection

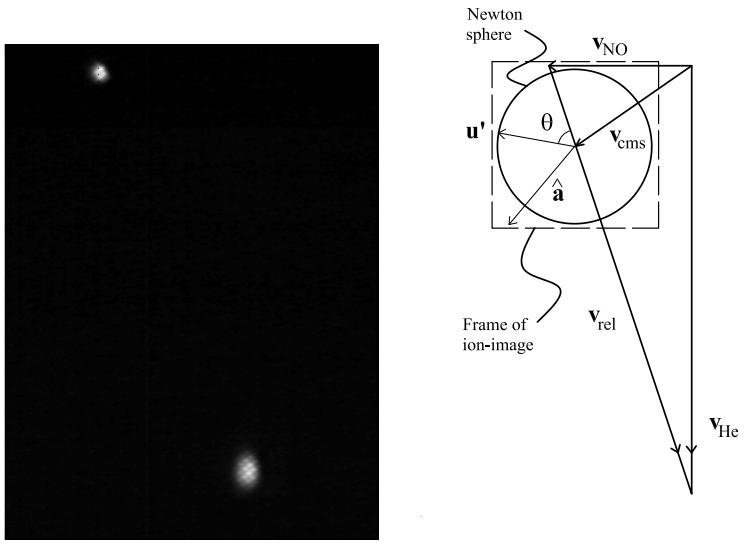

Figure 4. The left panel shows an ion image of two "beam spots". The top left spot is from the 16 % NO beam in Ar beam (593 m/s), while the lower spot is due to the 1 % NO in He beam velocity (1710 m/s). The camera is positioned such that the up-down direction of the ion-images coincides with the axis of the He beam, the left-right direction coincides with that of the NO beam. The right panel shows the corresponding Newton diagram. The vector $\mathbf{u}'$ indicates scattering with a velocity u' in the center-of-mass frame under an angle θ. The corresponding kinematic apse direction is indicated by $\hat{\mathbf{a}}$. Note that the u' distribution after collision is (cylindrically) symmetric around the relative velocity $\mathbf{v_{rel}}$. The dashed square indicates the frame of the recorded ion images that remains unaltered for all images in Fig. 5.

volume, and the blurring of the images are explicitly taken into account. An empirical blurring factor is used to make the simulated images as sharp as the experimental ones. To correct for the collision-induced rotational alignment, the assumption is used that the projection m_a of the rotational angular momentum $\mathbf{j}$ on the kinematic apse is conserved. The alignment dependent correction accounts for the (partial) saturation.

RESULTS AND DISCUSSION

In Fig. 5, the ion images are given for parity conserving and for parity breaking transitions, with j' ranging from $1\frac{1}{2}$ till $12\frac{1}{2}$. The images are grouped pairwise into parity pairs, see (11). The image for odd parity and $j = 9\frac{1}{2}$ could not be obtained because of two overlapping spectral lines. From these ion images the corresponding differential cross-sections are obtained. These are depicted in Fig. 6 and Fig. 7 together with the exact numerical results from the close coupling program HIBRIDON [27] and the approximate numerical results from our QQT theory. The differential cross-sections are plotted in units of Å^2 as a function of the angle θ. The total cross-sections of the experimental results and of the QQT results are normalized to those of the HIBRIDON calculations. The ratio of the total cross-section of the HIBRIDON calculation and the total cross-section of the QQT calculation, σ_H/σ_Q, is given above each subfigure.

For small values of j' the HIBRIDON results show diffraction effects at forward scattering angles. The experiment cannot resolve these fast oscillating diffraction peaks. The QQT calculations give a zero cross-section for the smallest angles. This is to be expected, since the diffraction effects are not incorporated into the QQT calculations; in the QQT approach a minimum amount of momentum transfer is needed. For higher values of j' the diffraction is no longer important, and the experimental results agree very well with the HIBRIDON calculations. The angular dependence of the QQT calculations is close to that of the other results. For the smallest values of j' the total cross-sections from the QQT calculations are less than half as large as those from the HIBRIDON calculations. This can be attributed to the absence of diffraction effects in the QQT calculations as mentioned before. Another reason is the hard shell approximation used in the current QQT calculations. A soft shell, and especially one including the small attractive component, will have a larger cross-section, especially for glancing collisions. For the largest values of j' the total cross-sections from the QQT calculations are between a factor of 3 and a factor of 10 larger than those from the HIBRIDON calculations. This can perhaps be (partly) explained by the fact that we do not take into account the spin orbit changing transitions.

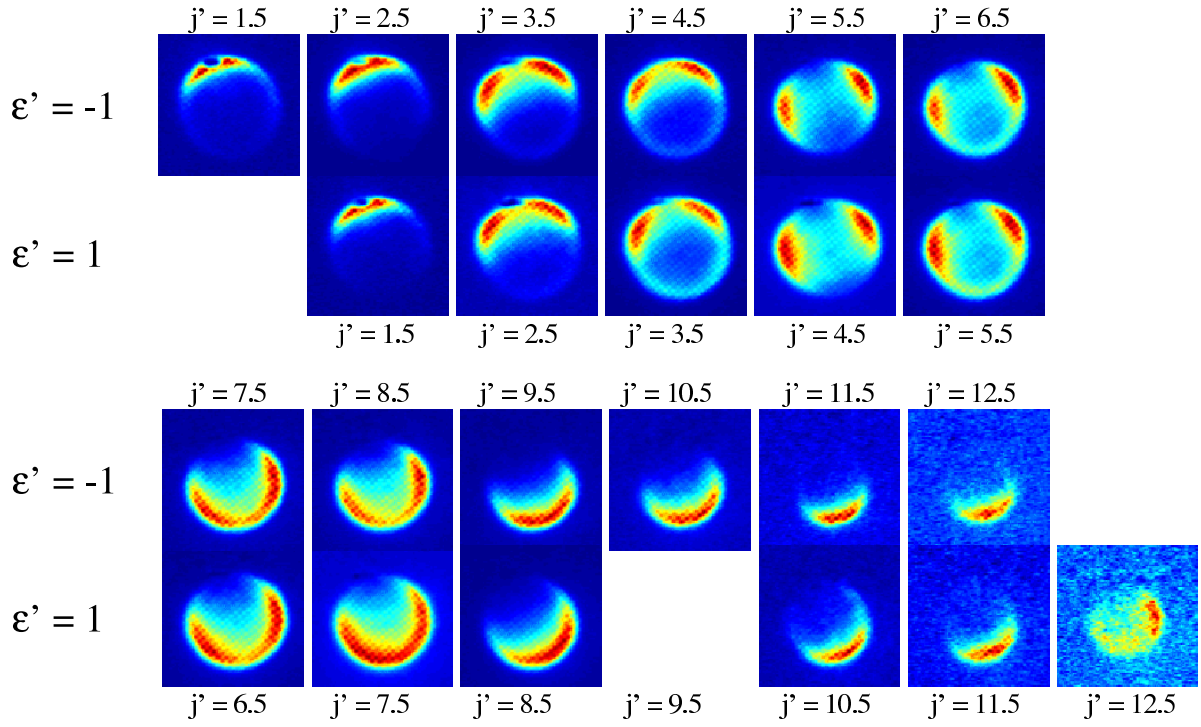

Figure 5. Ion images for He-NO collisions at $E_{tr} = 514\ cm^{-1}$. The parity pairs are grouped and separated from the other images by white lines. The image for $p' = -1$, $j' = 9.5$ could not be obtained because of two overlapping spectral lines. Images for $p' = 1$, $j' = 6.5$ and $p' = 1$, $j' = 7.5$ form a pair as well although they are displayed on different rows.

One can see that the maximum of the differential cross-sections shifts to larger scattering angles for larger values of j'. This change of the position of the maximum of the differential cross-section as a function of j' can be explained qualitatively as follows. Given j', ε' the parity pair number n is fixed. At forward scattering there is hardly any transfer of momentum possible and therefore no energy is available to excite a rotational level. Going to larger scattering angles the amount of momentum available for transfer is rising. From a certain scattering angle onwards the energy is available to make the transition to j'. For larger scattering angles the kinematic apse will become larger and so will the range of eta (as function of gamma), see (7). This means that the number of periods of $e^{i\eta(\gamma_a;\beta)}$ as a function of γ_a will rise. As a result the overlap with the Legendre polynomial of order n in (11) will rise too, until the maximum is reached.

From the differential cross-sections in Fig. 6 and Fig. 7, one can easily recognize the parity pairs. The differential cross-sections that form a parity pair can be plotted in the same figure. This is done for the experimental results in [5]. It shows that the match is very good.

CONCLUDING REMARKS

The QQT approach turns out to be remarkably accurate considering the crude approximations involved. In addition it provides physical insight into for example the position of the maximum of the differential cross-sections. In principle a lot of the framework of the QQT approach can be extended to use a soft shell representation of the intermolecular potential. It will be interesting to see whether this will result in a better match between the QQT approach and the close coupling calculations.

Looking further into the future we expect the QQT to provide reliable predictions - without much numerical effort - for the energy transfer in molecule-molecule collisions at thermal energies for systems like NO-N2 or N2-O2, which are still beyond reach of exact calculations.

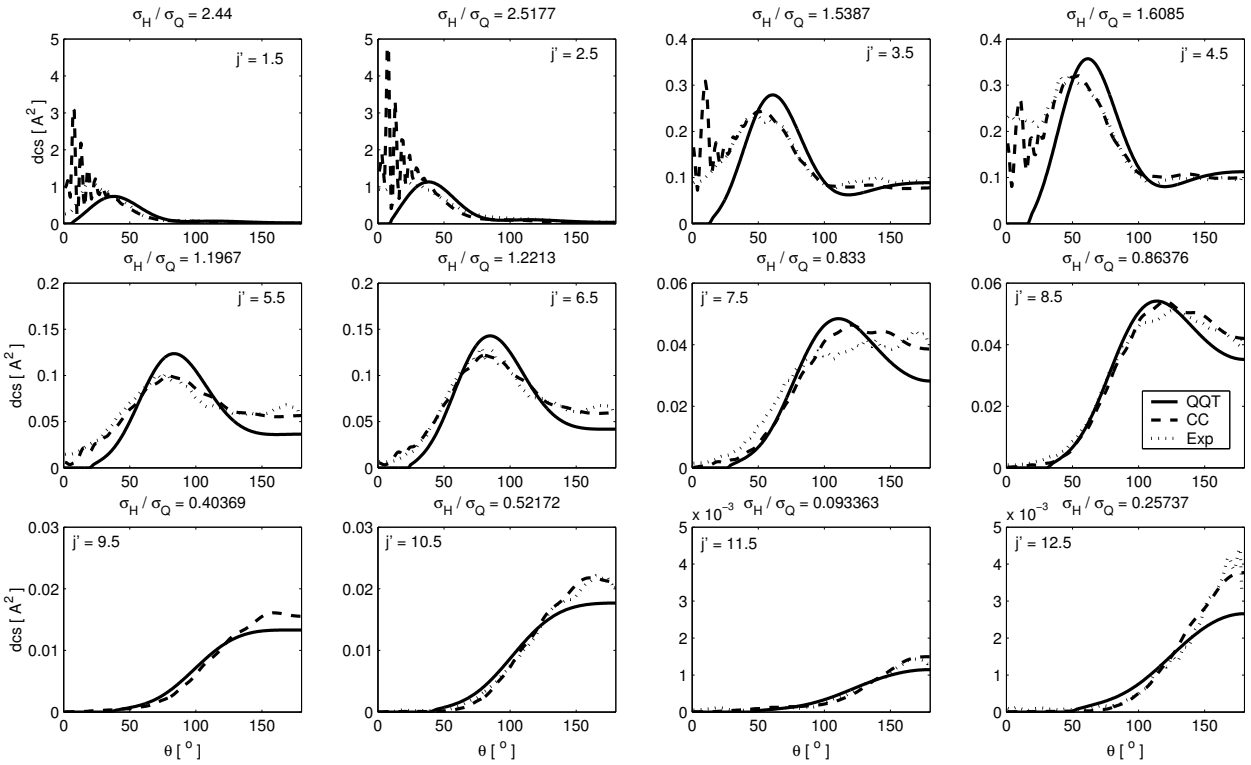

Figure 6. The differential cross sections for the parity conserving transitions ($p = p' = -1$). The parity pairs are easily seen in this figure. Both the experimental and the QQT results are normalized on the total cross section from the close coupling HIBRIDON results.

ACKNOWLEDGEMENTS

This work is part of the research program of the "Stichting voor Fundamenteel Onderzoek der Materie (FOM)", which is financially supported by the "Nederlandse Organisatie voor Wetenschappelijk Onderzoek (NWO)". C.A.T. is supported by the Division of Chemical Sciences, Geosciences and Biosciences, the Office of Basic Energy Sciences, the U. S. Department of Energy. Sandia is a multi-program laboratory operated by Sandia Corporation, a Lockheed Martin Company, for the National Nuclear Security Administration under contract DE-AC04-94-AL85000.

REFERENCES

1. R. D. Levine, *Reaction Dynamics* (Cambridge University Press, Cambridge, 2005).
2. A. Gijsbertsen, H. Linnartz, S. Stolte, and C. A. Taatjes, J. Am. Chem. Soc. **128**, 8777 (2006).
3. M. J. L. de Lange, S. Stolte, C. A. Taatjes, J. Kłos, G. C. Groenenboom, and A. v.d. Avoird, J. Chem. Phys. **121**, 11691 (2004).
4. J. L. van Leuken, J. Bulthuis, S. Stolte, and J. G. Snijders, Chem. Phys. Lett. **260**, 595 (1996).
5. A. Gijsbertsen, H. Linnartz, and S. Stolte, *In Press* (2006).
6. A. Gijsbertsen, H. Linnartz, G. Rus, A. E. Wiskerke, S. Stolte, D. W. Chandler, and J. Kłos, J. Chem. Phys. **123**, 224305 (2005).
7. G. Groenenboom (2005), private communications.
8. V. Khare, D. J. Kouri, and D. K. Hoffmann, J. Chem. Phys. **74**, 2275 (1981).
9. V. Khare, D. J. Kouri, and D. K. Hoffmann, J. Chem. Phys. **76**, 4493 (1982).
10. D. K. Hoffman, J. Chem. Phys **50**, 4823 (1969).
11. G. T. Evans, R. S. C. She, and R. B. Bernstein, J. Chem. Phys. **682**, 2258 (1985).
12. R. S. C. She, G. T. Evans, and R. B. Bernstein, J. Chem. Phys. **84**, 2204 (1986).
13. M. S. Child, *Molecular Collision Theory* (Dover Mineola NY, 1996).
14. D. J. Kouri and D. K. Hoffman, Theor. Chem. Acc. **103**, 281 (2000).
15. M. H. Alexander and S. Stolte, J. Chem. Phys. **112**, 8017 (2000).

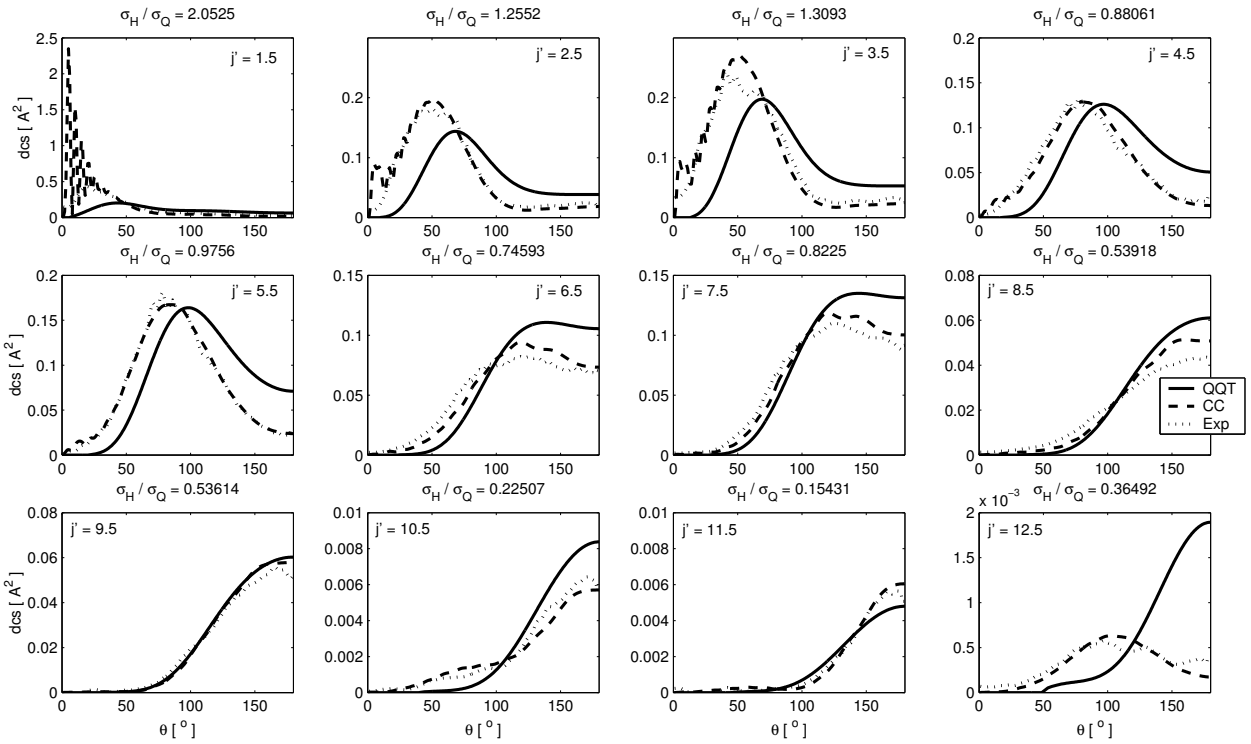

Figure 7. The differential cross sections for the parity breaking transitions ($p = -p'$). The parity pairs are easily seen in this figure. Both the experimental and the QQT results are normalized on the total cross section from the close coupling HIBRIDON results.

16. A. T. J. B. Eppink and D. H. Parker, Rev. Sci. Instrum. **68**, 3477 (1997).
17. K. T. Lorenz, M. S. Westley, and D. W. Chandler, Phys. Chem. Chem. Phys **2**, 481 (2000).
18. N. Yonekura, C. Gebauer, H. Kohguchi, and T. Suzuki, Rev. Sci. Instr. **70**, 2365 (1999).
19. A. A. Dixit, P. J. Pisano, and P. L. Houston, J. Phys. Chem. A **105**, 11165 (2001).
20. K. T. Lorenz, D. W. Chandler, J. W. Barr, W. Chen, G. L. Barnes, and J. I. Cline, Science **293**, 2063 (2001).
21. M. S. Elioff and D. W. Chandler, J. Chem. Phys. **117**, 6455 (2002).
22. M. S. Elioff, J. J. Valentini, and D. W. Chandler, Science **302**, 1940 (2003).
23. E. A. Wade, K. T. Lorenz, D. W. Chandler, J. W. Barr, G. L. Barnes, and J. I. Cline, Chem. Phys. **301**, 1 (2004).
24. T. P. Rakitzis, A. J. van den Brom, and M. H. M. Janssen, Science **303**, 1852 (2004).
25. B. Whitaker, ed., *Imaging in Molecular Dynamics* (Cambridge University press, Cambridge, 2003).
26. A. E. Wiskerke, C. A. Taatjes, A. W. Kleyn, R. J. W. E. Lahaye, S. Stolte, D. K. Bronnikov, and B. E. Hayden, Faraday Discussions **96**, 297 (1993).
27. HIBRIDON is a package of programs for the time independent quantum treatment of inelastic collisions written by M. H. Alexander, D. E. Manolopoulos, H.J. Werner, and B. Follmeg, with contributions by P. F. Vohralik, D. Lemoine, G. Corey, R. Gordon, B. Johnson, T. Orlikowski, A. Berning, A. Degli-Esposti, C. Rist, P. Dagdigian, B. Pouilly, G. van der Sanden, M. Yang, F. de Weerd, and S. Gregurick. More information and a copy of the code can be obtained from http://www.chem.umd.edu/physical/alexander/hibridon/.